

Article

Predictions for Bottomonia Suppression in 5.023 TeV Pb-Pb Collisions

Brandon Krouppa and Michael Strickland *

Department of Physics, Kent State University, Kent, OH 44242, USA; bkrouppa@kent.edu

* Correspondence: mstrick6@kent.edu

Academic Editor: name

Received: 5 August 2016; Accepted: 17 August 2016; Published: date

Abstract: We compute the suppression of the bottomonia states $Y(1S)$, $Y(2S)$, $Y(3S)$, $\chi_b(1P)$, $\chi_b(2P)$, and $\chi_b(3P)$ states in Large Hadron Collider (LHC) $\sqrt{s_{NN}} = 5.023$ TeV Pb-Pb collisions. For the background evolution we use 3+1d anisotropic hydrodynamics with conditions extrapolated from $\sqrt{s_{NN}} = 2.76$ TeV and we self-consistently compute bottomonia decay rates including non-equilibrium corrections to the interaction potential. For our final results, we make predictions for R_{AA} as function of centrality, rapidity, and p_T for the $Y(1S)$ and $Y(2S)$ states, including feed down effects. In order to assess the dependence on some of the model assumptions, we vary the shear viscosity-to-entropy density ratio, $4\pi\eta/s \in \{1, 2, 3\}$, and the initial momentum-space anisotropy parameter, $\xi_0 \in \{0, 10, 50\}$, while holding the total light hadron multiplicity fixed.

Keywords: relativistic heavy ion collisions; quarkonium suppression

1. Introduction

Ultra-relativistic heavy ion collisions (URHICs) carried out at the Large Hadron Collider (LHC) at CERN and the Relativistic Heavy Ion Collider (RHIC) at Brookhaven National Laboratory create super-hot and dense matter. The observed thermal particle spectra and anisotropic collective flow seen in such collisions has been taken as evidence of the creation of a deconfined high-temperature quark-gluon plasma (QGP). The existence of the QGP itself is a prediction of finite-temperature quantum chromodynamics (QCD), and the QGP is believed to have been the state of the early universe.

Comparisons between theory and experiment suggest that LHC URHICs produce a QGP with an initial temperature on the order of $T_0 = 500$ – 600 MeV for $\sqrt{s_{NN}} = 2.76$ TeV Pb-Pb collisions [1,2]. The LHC has recently performed URHICs with nucleon–nucleon center-of-mass energies of $\sqrt{s_{NN}} = 5.023$ TeV, which are expected to produce initial temperatures on the order of $T_0 = 600$ – 700 MeV. Analysis of collective flow data indicate that the QGP behaves like a nearly-perfect fluid with shear viscosity-to-entropy density ratio η/s approaching the conjectured lower bound of $1/(4\pi)$. Despite being nearly ideal, one complication that must be faced is that, although the QGP is close to thermal equilibrium at late times, URHICs produce a QGP which is momentum-space anisotropic in the local rest frame with the degree of momentum-space anisotropy decreasing slowly as a function of proper time. This can have an impact on the various signatures for QGP formation, such as heavy quarkonium suppression [3,4].

Heavy quark-bound states are of particular interest because they can survive into the deconfined phase due to their large binding energy. They are expected to survive up to a few times the pseudo-critical temperature, T_c ; however, at sufficiently high temperatures, even heavy quark bound states should disassociate. As a result, in the late 1980's Karsch, Matsui, Mehr, and Satz predicted that heavy quark–antiquark bound states, known as quarkonia, would be suppressed in heavy ion collisions compared to proton–proton (p-p) collisions [5,6]. The resulting suppression of heavy quarkonia can be used to probe the entire history of the QGP, since heavy quarkonium states are produced early

in the QGP evolution. There has been a significant amount of work dedicated to the study of heavy quarkonia suppression. For recent related work, see References [7–10]. In this paper, we focus on bottomonia states which survive up to plasma temperatures of $T_d \sim 600, 230,$ and 170 MeV for $Y(1S), Y(2S),$ and $Y(3S)$ states, respectively [11]. At these temperatures, the in-medium width of the state becomes on the order of the real part of its binding energy, and the state quickly dissociates; however, prior to this disassociation point, the states have large widths (~ 50 – 100 MeV), with the widths for the excited states being larger than those for the ground state. As a consequence, one expects sequential melting of heavy bottomonia states in QGP, with excited states melting before the ground state, and lighter states dissociating before heavier states [12].

In this paper, we focus on bottomonia states since they can be more reliably treated using potential-based non-relativistic effective field theory (pNRQCD) [13–17]. We include the effect of in-medium disassociation in the presence of a complex-valued potential obtained using hard-thermal-loop perturbation theory [18–22]. We also take into account the non-equilibrium momentum-space anisotropy produced as a result of the rapid longitudinal expansion of the QGP via modifications to both the real and imaginary parts of the potential [23]. This work extends our previous work [24–26] to $\sqrt{s_{NN}} = 5.023$ TeV Pb-Pb collisions. As before, we use 3 + 1d anisotropic hydrodynamics (aHydro) for the background evolution [3,27–31].

For the $\sqrt{s_{NN}} = 5.023$ TeV initial conditions, we extrapolate the initial conditions used at lower collision energies and make predictions for the inclusive R_{AA} for the $Y(1S)$ and $Y(2S)$ states, including feed down contributions. To assess the dependence on some of the model assumptions, we vary the shear viscosity-to-entropy density ratio, $4\pi\eta/s \in \{1, 2, 3\}$, and the initial momentum-space anisotropy parameter, $\xi_0 \in \{0, 10, 50\}$, while holding the total light hadron multiplicity fixed.

2. 3 + 1d Anisotropic Hydrodynamics

In aHydro, the local rest frame (LRF) partonic distribution is assumed to be of the form [27,28,32]

$$f(p, x) = f_{\text{eq}} \left(\sqrt{p_T^2 + [1 + \xi(x)]p_z^2} / \Lambda(x) \right), \quad (1)$$

where $-1 \leq \xi(x) < \infty$ is the local momentum-space anisotropy parameter, $\Lambda(x)$ is the local transverse temperature of the plasma, and f_{eq} is an arbitrary isotropic equilibrium distribution function which here we take to be a Boltzmann distribution. The local anisotropy $\xi(x)$ encodes the viscous corrections to an ideal isotropic QGP. Note that, in the most recent applications of aHydro, one allows for the existence of three independent anisotropy parameters; see e.g., Reference [30]. This takes into account both bulk and shear viscous effects in the QGP. In this paper, we use the simpler “one anisotropy parameter” version. This is sufficient for our purposes, since the additional anisotropy parameters are small and, therefore, subleading. For details concerning the aHydro dynamical equations and the numerical methods used, see References [33,34].

We start the hydrodynamic evolution of the system at $\tau_0 = 0.3$ fm/c. For the initial conditions, we use the Glauber model with a linear combination of wounded-nucleon and binary collisions. The fraction of the binary collision component is taken to be $\kappa_{\text{binary}} = 0.145$. The inelastic cross-section for $\sqrt{s_{NN}} = 2.76$ TeV collisions is taken to be $\sigma_{NN}^{2.76 \text{ TeV}} = 62$ mb, while for $\sqrt{s_{NN}} = 5.023$ TeV collisions, we extrapolate from the results presented in Reference [35] to obtain $\sigma_{NN}^{5.023 \text{ TeV}} = 67$ mb. In both cases, we use a standard Woods–Saxon profile for the incoming nuclei with $n_A(r) = n_0 / (1 + e^{(r-R)/d})$, where $n_0 = 0.17 \text{ fm}^{-3}$ is the central nucleon density and is determined via the normalization $\lim_{A \rightarrow \infty} \int d^3r n_A(r) = A$, $R = (1.12A^{1/3} - 0.86A^{-1/3})$ fm is the nuclear radius, and $d = 0.54$ fm is the skin depth of the nucleus [36].

The initial longitudinal profile is approximated by distribution featuring a nearly boost-invariant plateau region for mid-rapidities and a tail characterized by a Gaussian which reflects limiting fragmentation [37]

$$\mathcal{F}(\zeta) \equiv \exp \left[-\frac{(\zeta - \Delta_\zeta)^2}{2\sigma_\zeta^2} \Theta(|\zeta| - \Delta_\zeta) \right]. \tag{2}$$

For $\sqrt{s_{NN}} = 2.76$ TeV collisions, fits were made to experimental particle pseudorapidity profiles which give $\Delta_\zeta^{2.76 \text{ TeV}} = 2.5$ and $\sigma_\zeta^{2.76 \text{ TeV}} = 1.4$. For $\sqrt{s_{NN}} = 5.023$ TeV collisions, we use the predictions of Reference [38], which determined the rapidity profile in the high energy limit. Using the results of Reference [38], one finds that going from 2.76 TeV collisions to 5.023 TeV collisions, there is an approximately 12% increase in plateau halfwidth, which gives $\Delta_\zeta^{5.023 \text{ TeV}} = 2.8$. Based on [38], we found no observable change of the Gaussian halfwidth in 5.023 TeV collisions, and therefore we take $\sigma_\zeta^{5.023 \text{ TeV}} = 1.4$. The combination of Glauber in the transverse plane and the longitudinal profile function above gives us the full 3d initial energy density profile for the QGP.

The initial plasma temperatures, T_0 , for 2.76 TeV collisions are taken from our previous work [24] and are consistent with the analysis of elliptic flow coefficients [39]. In Table 1, we show the initial conditions used at 2.76 TeV. The values in the center of Tables 1 and 2 are the initial transverse temperatures of the plasma, which enter into the one-particle distribution function, Equation (1). Note that unless $\zeta_0 = 0$, the transverse temperature cannot be interpreted as temperature. The entry with $\zeta_0 = 0$ and $4\pi\eta/s = 1$ was obtained via fits to collective flow, and the other entries were obtained by varying either ζ_0 or η/s while holding the total particle multiplicity fixed. Note that, when $\zeta_0 \neq 0$, we set the initial condition for the transverse temperature Λ_0 instead of the initial temperature due to the momentum-space anisotropy.

Table 1. Λ_0 values for 2.76 TeV collisions in GeV.

$4\pi\eta/s \backslash \zeta_0$	0	10	50
1	0.552	0.765	0.925
2	0.546	0.752	0.909
3	0.544	0.748	0.906

For 5.023 TeV collisions, we assume that the temperature of the plasma scales proportionally with the fourth root of the collision energy—i.e., $T_0 \propto s_{NN}^{1/8}$. Using this assumption, we predict a 16% increase in the initial central temperature when going from 2.76 TeV to 5.023 TeV collisions. We apply this scaling to the 2.76 TeV initial conditions with $\zeta_0 = 0$ and $4\pi\eta/s = 1$ and then, as before, we fill out the rest of the initial conditions table by holding the total particle multiplicity fixed. The resulting table of initial conditions is shown in Table 2.

Table 2. Λ_0 values for 5.023 TeV collisions in GeV.

$4\pi\eta/s \backslash \zeta_0$	0	10	50
1	0.641	0.888	1.076
2	0.632	0.869	1.053
3	0.629	0.863	1.046

3. Model Potential

Modeling bottomonia states in a QGP which is anisotropic in momentum-space requires going beyond the Karsch, Matsui, Mehr, and Satz model which describes the free energy of a static heavy quark–antiquark pair in an isotropic plasma. It has been shown in References [7,25] that free-energy-based potential models of the quarkonium pair do not agree with experimental R_{AA} data.

For this reason, we use the internal energy of the bottomonia pair $U = F + TS$ to provide the model potential. The masses of heavy quarks allow bottomonia pairs to be treated using pNRQCD methods which allow us to systematically include relativistic corrections. We use a model which represents the short- and medium-range gluonic screening of the heavy-quark potential in a momentum-space anisotropic plasma [19,21,22,25,26]. For the long range real part of the potential, we use the original Karsh–Mehr–Satz (KMS) form for the free energy. The resulting internal-energy-based model has the following form for the real part of the heavy quark potential

$$\Re[V] = -\frac{a}{r}(1 + \mu r)e^{-\mu r} + \frac{2\sigma}{\mu}[1 - e^{-\mu r}] - \sigma r e^{-\mu r} - \frac{0.8\sigma}{m_b^2 r}, \tag{3}$$

where $\mu = \mathcal{G}(\zeta, \theta)m_D$ [19,22,25], with θ being the angle between the line connecting the quark–antiquark pair and the beam-line direction, m_D is the isotropic leading-order Debye mass, $a = 0.385$, $\sigma = 0.223 \text{ GeV}^2$ [40], and $m_b = 4.7 \text{ GeV}$ is the mass of the bottom quark. The last term taken from Reference [41] accounts for the temperature- and spin-independent finite-quark-mass correction, to obtain our final complex-valued potential (This term is not particularly important for bottomonia states. We include it for historical continuity with our previous works, where we also considered charmonium suppression). For the imaginary part of the potential, we use a small- ζ expansion of the heavy-quark potential [18,20,21]

$$\Im[V] = -\alpha_s C_F T \left\{ \phi(\hat{r}) - \zeta [\psi_1(\hat{r}, \theta) + \psi_2(\hat{r}, \theta)] \right\}, \tag{4}$$

where $\hat{r} = r m_D$, $\phi(\hat{r})$ is defined as

$$\phi(\hat{r}) = 2 \int_0^\infty dz \frac{z}{(z^2 + 1)^2} \left[1 - \frac{\sin(z\hat{r})}{\hat{r}} \right], \tag{5}$$

and ψ_1 and ψ_2 are defined as follows

$$\psi_1(\hat{r}, \theta) = \int_0^\infty dz \frac{z}{(z^2 + 1)^2} \left(1 - \frac{3}{2} \left[\sin^2 \theta \frac{\sin(z\hat{r})}{z\hat{r}} + (1 - 3 \cos^2 \theta) G(\hat{r}, z) \right] \right), \tag{6}$$

$$\psi_2(\hat{r}, \theta) = - \int_0^\infty dz \frac{\frac{4}{3}z}{(z^2 + 1)^3} \left(1 - 3 \left[\left(\frac{2}{3} - \cos^2 \theta \right) \frac{\sin(z\hat{r})}{z\hat{r}} + (1 - 3 \cos^2 \theta) G(\hat{r}, z) \right] \right). \tag{7}$$

The algorithm from Reference [23,42] is used to solve the resulting 3d Schrödinger equation on a regular lattice by transforming to imaginary time and using the finite difference time domain (FDTD) method. Using this method, we compute the real and imaginary parts of the binding energy over a range of Λ from 144 MeV to 1037 MeV. For each Λ , we compute the real and imaginary binding energies for a range of anisotropies, ζ , from -0.3 to 200, with an irregular spacing which accounts for the fact that the majority of the time the system probes small values of ζ . We use a $N^3 = 256^3$ lattice with lattice spacing $a = 0.1 \text{ GeV}^{-1} \approx 0.02 \text{ fm}$ and $a = 0.15 \text{ GeV}^{-1} \approx 0.03 \text{ fm}$ for a total box length of $L = Na \approx 5.04 \text{ fm}$ and $L = Na \approx 7.56 \text{ fm}$, for Y and χ_b states, respectively. The imaginary-time step size for the algorithm is taken to be $\Delta\tau = a^2/8$.

The real and imaginary binding energies are extracted using [25]

$$E_{\nu, \text{bind}} \equiv - \left(E_\nu - m_1 - m_2 - \frac{\langle \phi_\nu | V_\infty(\theta) | \phi_\nu \rangle}{\langle \phi_\nu | \phi_\nu \rangle} \right), \tag{8}$$

where

$$V_\infty(\theta) \equiv \lim_{|\mathbf{r}| \rightarrow \infty} \Re[V(\theta, \mathbf{r})]. \tag{9}$$

Negative values of $\Im[E_{\text{bind}}]$ only occur for large values of ξ , which is a consequence of the small- ξ expansion. Large values of ξ correspond to a nearly free streaming quark-gluon plasma, so it is expected that the widths of bottomonia states return to vacuum values, which are on the order of $\sim \text{keV}$, which effectively allows us to set $\Im[E_{\text{bind}}] = 0$ for this specific case.

4. Bottomonium Suppression

We use the following rate equation to account for in-medium bottomonia state decay,

$$\frac{dn(\tau, \mathbf{x}_\perp, \zeta)}{d\tau} = -\Gamma(\tau, \mathbf{x}_\perp, \zeta)n(\tau, \mathbf{x}_\perp, \zeta), \quad (10)$$

where all variables depend on longitudinal proper time $\tau = \sqrt{t^2 - z^2}$, the transverse coordinate \mathbf{x}_\perp , and the spatial rapidity $\zeta = \text{arctanh}(z/t)$. The rate of decay is computed by [25]

$$\Gamma(\tau, \mathbf{x}_\perp, \zeta) = \begin{cases} 2\Im[E_{\text{bind}}(\tau, \mathbf{x}_\perp, \zeta)] & \Re[E_{\text{bind}}(\tau, \mathbf{x}_\perp, \zeta)] > 0 \\ \gamma_{\text{dis}} & \Re[E_{\text{bind}}(\tau, \mathbf{x}_\perp, \zeta)] \leq 0. \end{cases} \quad (11)$$

where γ_{dis} is a large value which is chosen such that a completely unbound state decays quickly. We emphasize that E_{bind} and hence Γ are local quantities of τ , \mathbf{x}_\perp , and ζ through the 3 + 1d background evolution of the transverse temperature $\Lambda(x)$ and the local momentum-space anisotropy $\xi(x)$.

4.1. Survival Probability

The survival probability is determined by integrating Equation (10) over proper time with the integration limits set dynamically. The lower integration limit for the proper-time integration is $\max(\tau_{\text{form}}, \tau_0)$, where τ_0 is the initial proper time for plasma evolution and τ_{form} is the time-dilated formation time of the state in question, computed via $\tau_{\text{form}}(p_T) = \gamma \tau_{\text{form}}^0 = E_T \tau_{\text{form}}^0 / M$, where M is the mass of the state. The rest-frame formation time τ_{form}^0 for each of the states is taken to be inversely proportional to the vacuum binding energy of each state [43], and thus, $\tau_{\text{form}}^0 = 0.2, 0.4, 0.6, 0.4, 0.6$, and $0.6 \text{ fm}/c$, for $Y(1S)$, $Y(2S)$, $Y(3S)$, $\chi_b(1P)$, $\chi_b(2P)$, and $\chi_b(3P)$, respectively. The upper limit for the proper-time integration is determined to be the proper time at which the local energy density becomes less than the energy density of an $N_c = 3$ and $N_f = 2$ ideal gas of quarks and gluons with a temperature of $T_f = 192 \text{ MeV}$. This is the temperature at which screening effects are assumed to turn off rapidly due to the transition to the hadronic phase.

Transverse momentum cuts were implemented by assuming that the transverse momentum distribution of bottomonia states is proportional to E_T^{-4} ,

$$R_{AA}(\mathbf{x}_\perp, \zeta) \equiv \frac{\int_{p_{T,\text{min}}}^{p_{T,\text{max}}} dp_T^2 R_{AA}(p_T, \mathbf{x}_\perp, \zeta) / (p_T^2 + M^2)^2}{\int_{p_{T,\text{min}}}^{p_{T,\text{max}}} dp_T^2 / (p_T^2 + M^2)^2}. \quad (12)$$

Once the transverse momentum cut is applied, we average R_{AA} over the transverse plane

$$\langle R_{AA}(\zeta) \rangle \equiv \frac{\int_{\mathbf{x}_\perp} n_{AA}(\mathbf{x}_\perp) R_{AA}(\mathbf{x}_\perp, \zeta)}{\int_{\mathbf{x}_\perp} n_{AA}(\mathbf{x}_\perp)}, \quad (13)$$

where $T_A(x, y) = \int_{-\infty}^{\infty} dz n_A(\sqrt{x^2 + y^2 + z^2})$ is the nuclear thickness function and $n_{AB} = T_A(x + b/2, y)T_B(x - b/2, y)$ is the overlap density function. In the above relations, it is assumed that n_{AA} sets the probability for bottomonia production at a given point in the transverse plane. After the p_T cuts and spatial averaging are performed, centrality averaging is performed by converting the impact parameter, b , to centrality, C , using the Glauber model, and then integrating over the centrality cut with a probability distribution proportional to $e^{-C/20}$ with $0 < C < 100$ [44].

4.2. Excited State Feed Down

A certain fraction of $Y(1S)$ and $Y(2S)$ states produced in URHICs are formed via the decay of excited states. To compute the post feed down R_{AA} for the $Y(1S)$ and $Y(2S)$ states, R_{AA} is computed taking into account the suppression of excited states which undergo late time feed down. For this purpose, we use p_T -averaged feed down fractions obtained recently from a compilation of p-p data available from ATLAS, CMS, and LHCb [45]. The fractions $f_i^{Y(1s)}$ and $f_i^{Y(2s)}$ are given in Tables 3 and 4, which specify the fraction of a particular state which contributes to the $Y(1S)$ and $Y(2S)$ states. The inclusive feed down R_{AA} of each of the states is calculated using a linear combination of the primordial R_{AA} using the respective feed down fractions $R_{AA}^{Y(nS)} = \sum_{i \in \text{states}} f_i^{Y(nS)} R_{AA,i}$, where $R_{AA,i}$ is the primordial suppression for the i th state.

Table 3. Feed down fractions to the $Y(1S)$ state.

Y(1S) Feed Down Fractions	
$Y(1S)$	0.668
$Y(2S)$	0.086
$Y(3S)$	0.010
$\chi_b(1P)$	0.170
$\chi_b(2P)$	0.051
$\chi_b(3P)$	0.015

Table 4. Feed down fractions to the $Y(2S)$ state.

Y(2S) Feed Down Fractions	
$Y(2S)$	0.604
$Y(3S)$	0.043
$\chi_b(2P)$	0.309
$\chi_b(3P)$	0.044

4.3. Results

We now turn to our results and predictions. In Figure 1, we show the “primordial” R_{AA} for the six states as a function of N_{part} for the case of $4\pi\eta/s = 1$. The primordial suppression is the result obtained prior to taking into account feed down effects. The left panel shows the result for $\sqrt{s_{NN}} = 2.76$ TeV, and the right panel shows our prediction for $\sqrt{s_{NN}} = 5.023$ TeV. From this figure, one can immediately see the sequential suppression of states, with excited states showing more suppression, which is a consequence of the lower dissociation temperatures compared to, for example, the $Y(1S)$ state. Going from 2.76 TeV to 5.023 TeV, we see increased primordial suppression for all states considered, with the “primordial” R_{AA} decrease by approximately 31%, 48%, 44%, 51%, 45%, and 44% for the $Y(1S)$, $Y(2S)$, $Y(3S)$, $\chi_b(1P)$, $\chi_b(2P)$, and $\chi_b(3P)$ states, respectively, for central collisions. Finally, we note that at both energies, the model predicts significant primordial suppression of the $Y(1S)$, even though the temperatures probed in the plasma are below the state’s disassociation temperature for most of the plasma evolution. The primordial suppression seen is a result of the fact that the decay rate remains large even below the naive disassociation temperature for a given state.

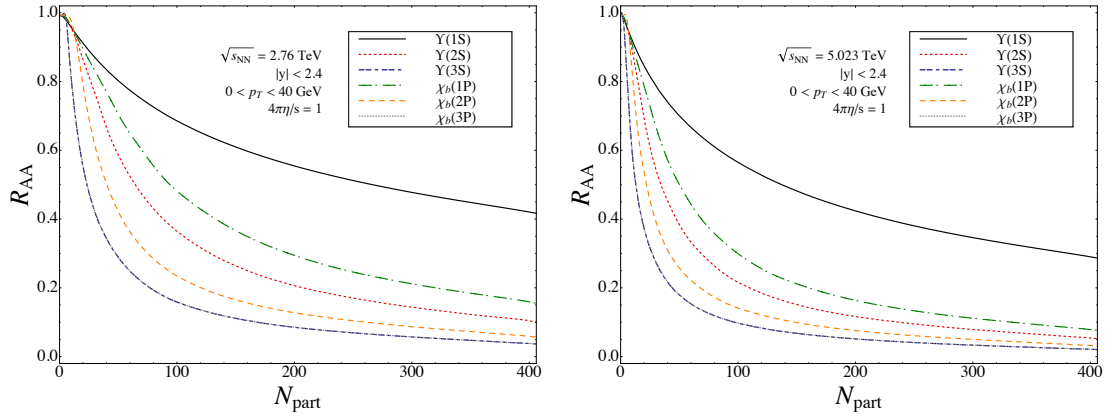


Figure 1. (Color online) Primordial R_{AA} for each modeled state as a function of the number of participants. Note that the suppression curves for the $Y(3S)$ and $\chi_b(3P)$ states fall on top of each other.

In Figure 2, we compare the inclusive suppression of the $Y(1S)$ state at 2.76 TeV and 5.023 TeV as a function of N_{part} . The inclusive R_{AA} includes the effect of resonance feed down. For Figure 2, we integrated over rapidity in the range $|y| < 2.4$ and transverse momentum in the range $0 < p_T < 40$ GeV. The top band (light blue) corresponds to $\sqrt{s_{NN}} = 2.76$ TeV, and the bottom band (light green) corresponds to $\sqrt{s_{NN}} = 5.023$ TeV. In each of the bands, the solid (black), short-dashed (red), and long-dashed (blue) lines correspond to $4\pi\eta/s \in \{1, 2, 3\}$. As this figure demonstrates, our model prediction is that one should see enhanced suppression of the $Y(1S)$ at $\sqrt{s_{NN}} = 5.023$ TeV compared to $\sqrt{s_{NN}} = 2.76$ TeV. For a central collision, we see an approximately 34% decrease in the $Y(1S)$ R_{AA} for $4\pi\eta/s = 1$.

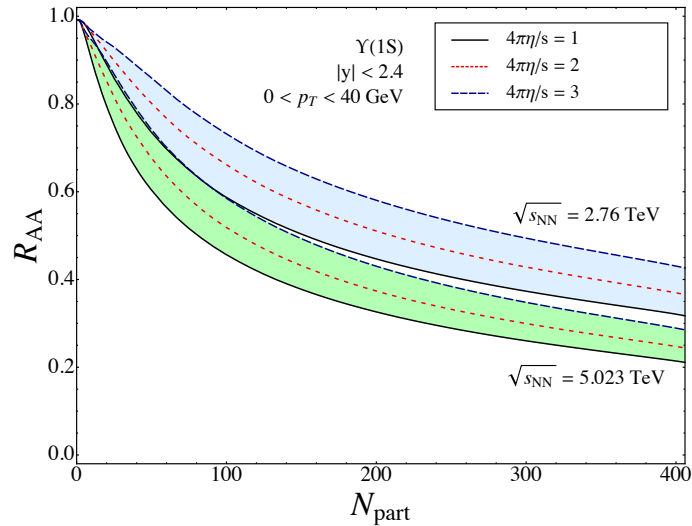


Figure 2. (Color online) Inclusive $Y(1S)$ state calculated with feed down contributions from excited states. Here we show a comparison between $\sqrt{s_{NN}} = 2.76$ TeV and $\sqrt{s_{NN}} = 5.023$ TeV collision energies.

In Figures 3 and 4, we compare the inclusive suppression of the $Y(1S)$ state at 2.76 TeV and 5.023 TeV as a function of p_T and y , respectively. The labelling and line types are the same as in Figure 2. Due to the large size of the experimental p_T bins, for Figure 3 we have binned our predictions into the experimental bins. From Figures 3 and 4, we find that the model once again predicts enhanced suppression of the $Y(1S)$ when going from 2.76 to 5.023 TeV as a function of p_T and y . In the lowest p_T bin, we predict a decrease in R_{AA} of approximately 25% for the case $4\pi\eta/s = 1$. For $|y| = 0$, we predict a decrease in R_{AA} of approximately 26% for the same case. We also note that there is a slight

increase in suppression for forward rapidities, which is due to the increased plateau halfwidth used in the initial conditions.

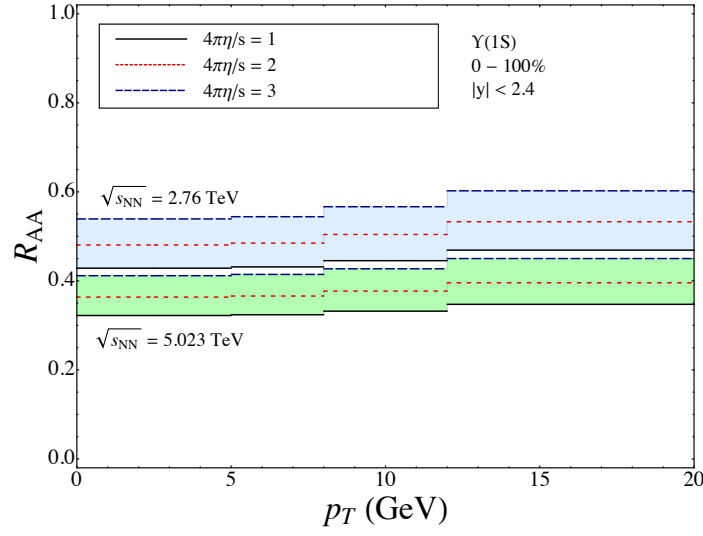


Figure 3. (Color online) Inclusive Y(1S) state calculated with feed down contributions from excited states. Here we show a comparison between $\sqrt{s_{NN}} = 2.76$ TeV and $\sqrt{s_{NN}} = 5.023$ TeV collision energies.

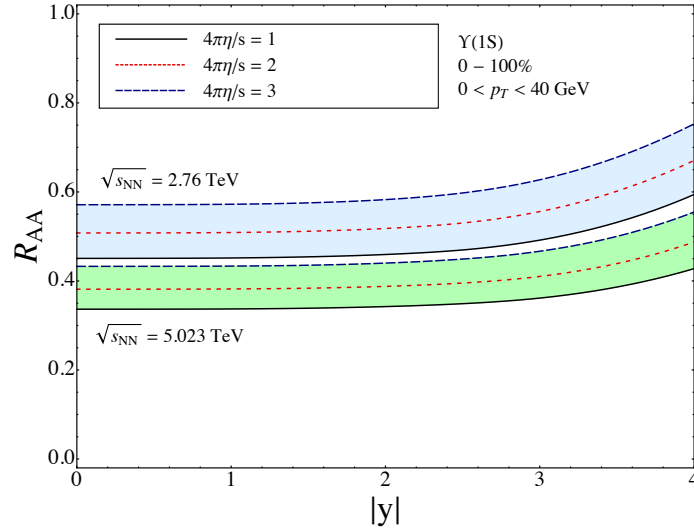


Figure 4. (Color online) Inclusive Y(1S) state calculated with feed down contributions from excited states. Here we show a comparison between $\sqrt{s_{NN}} = 2.76$ TeV and $\sqrt{s_{NN}} = 5.023$ TeV collision energies.

In Figures 5–7, we collect our predictions for the Y(1S) and Y(2S) inclusive R_{AA} for $\sqrt{s_{NN}} = 5.023$ TeV collision energy. The line styles are the same as in the previous figures. As can be seen from these figures, we also predict further suppression of the Y(2S) at $\sqrt{s_{NN}} = 5.023$ TeV as a function of N_{part} , p_T , and y . Finally, in Figure 8, we plot the inclusive Y(1S) suppression as a function of N_{part} for the case $4\pi\eta/s = 1$, but now varying the initial momentum-space anisotropy ξ_0 of the QGP. The solid (black) line shows the case $\xi_0 = 0$, which corresponds to a QGP that is perfectly isotropic at τ_0 . The short-dashed (red) line and long-dashed (blue) lines correspond to $\xi_0 = 10$ and $\xi_0 = 50$, respectively. The finite values of ξ_0 map to initial pressure anisotropies in the local rest frame of $\mathcal{P}_L/\mathcal{P}_T = 0.13$ and 0.03, respectively. The presence of an initial momentum-space anisotropy is

predicted by both weak and strong coupling approaches, with weak coupling approaches predicting larger initial momentum-space anisotropies than the strong coupling approaches [3,4].

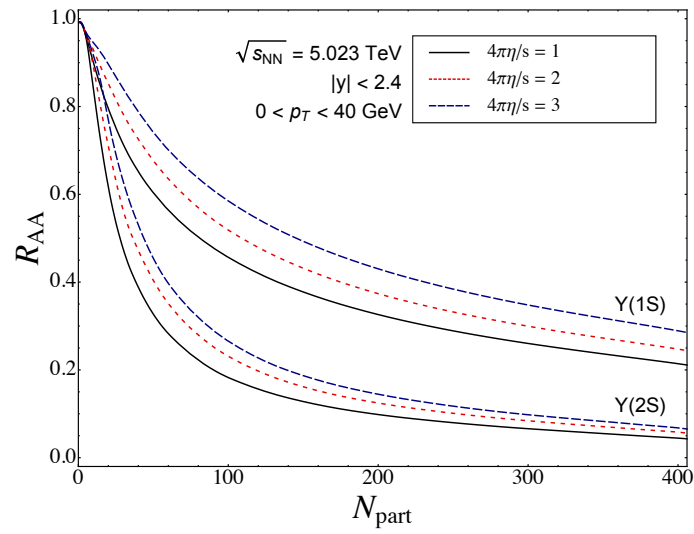


Figure 5. (Color online) Predictions for inclusive Y(1S) and Y(2S) suppression for $\sqrt{s_{NN}} = 5.023$ TeV Pb-Pb collisions.

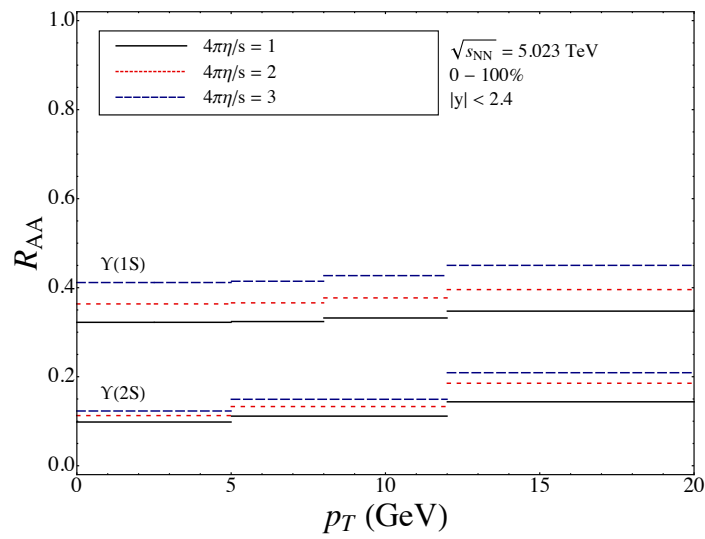


Figure 6. (Color online) Predictions for inclusive Y(1S) and Y(2S) suppression for $\sqrt{s_{NN}} = 5.023$ TeV Pb-Pb collisions.

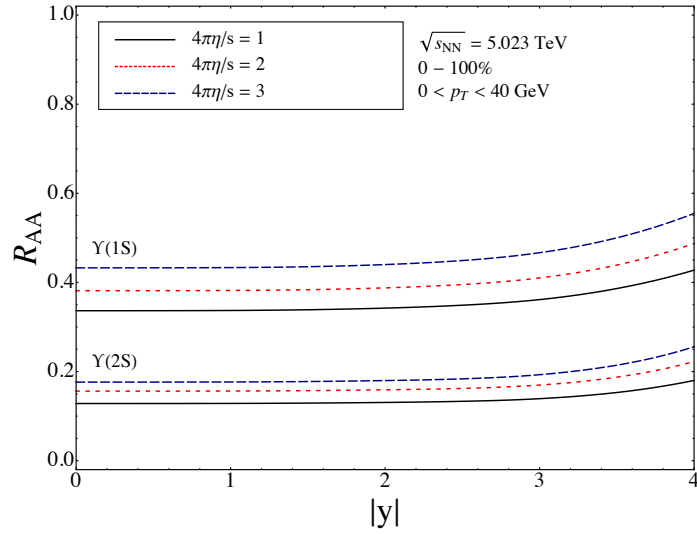


Figure 7. (Color online) Predictions for inclusive Y(1S) and Y(2S) suppression for $\sqrt{s_{NN}} = 5.023$ TeV Pb-Pb collisions.

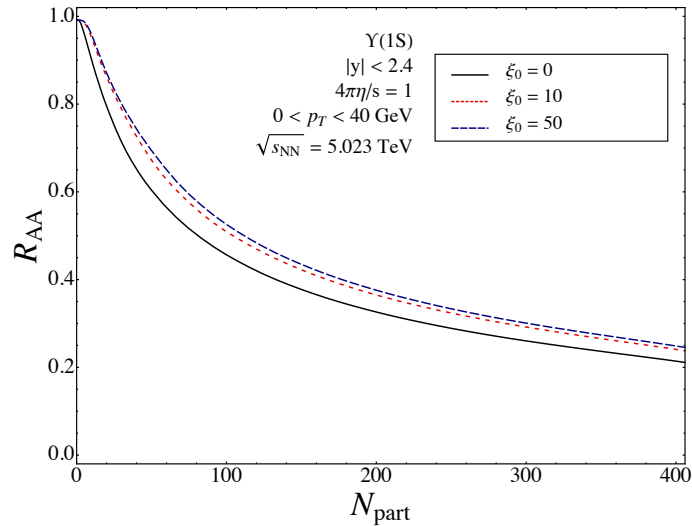


Figure 8. (Color online) Inclusive Y(1S) suppression for zero and finite initial anisotropy, ζ_0 .

As Figure 8 demonstrates, the effect of initial momentum-space anisotropy is to decrease the amount of Y(1S) suppression. Going from $\zeta_0 = 0$ to $\zeta_0 = 50$, we see an approximately 14% increase in the inclusive Y(1S) R_{AA} for a central collision. The effect of initial momentum-space anisotropy on the Y(2S) is qualitatively similar, however, the effect is larger. We find that the inclusive Y(2S) R_{AA} increases by approximately 27% for ζ_0 in the same range.

5. Conclusions

The primary goal of this work was to make predictions for bottomonia suppression at the latest LHC URHIC energy of $\sqrt{s_{NN}} = 5.023$ TeV. In order to make our predictions, we had to make some extrapolations of the initial conditions for the background. The key changes in going from 2.76 TeV to 5.023 TeV were a 16% increase in the initial central temperature, an increase in the width of the central rapidity plateau [38], and a small change in the nucleon–nucleon scattering cross section [35]. With these assumptions, we then made predictions with the same model employed in our prior works on this subject [24–26]. The model includes the effect of in-medium dissociation of bottomonia, uses a full 3 + 1d anisotropic viscous hydrodynamics background, and takes into account non-equilibrium

modifications of the heavy quark potential associated with large momentum-space anisotropy. We did not include any cold nuclear matter effects or regeneration, since these are expected to be small for the bottomonia states.

Comparing higher energy 5.023 TeV collisions to 2.76 TeV collisions, our model predicts that one should see enhanced suppression of bottomonia states as a function of centrality, transverse momentum, and rapidity. We have provided quantitative calculations of R_{AA} for both the $Y(1s)$ and $Y(2s)$, including feed down effects which can be compared with forthcoming data from the LHC.

Finally, in addition to extrapolating our results to the higher energy, we looked at the effect of initial momentum-space anisotropy on bottomonia suppression. For levels of momentum-space anisotropy predicted by theoretical models, we find an approximately 14% increase in the $Y(1s)$ inclusive R_{AA} . We plan to study this effect in more detail in the future, since it can affect the extracted value of η/s when comparing with experimental data.

Acknowledgments: M. Strickland and B. Krouppa were supported by the U.S. Department of Energy under Award No. DE-SC0013470.

Author Contributions: M. Strickland and B. Krouppa contributed to both the theoretical and numerical aspects of the work presented herein.

Conflicts of Interest: The authors declare no conflict of interest.

References

1. Heinz, U.; Snellings, R. Collective flow and viscosity in relativistic heavy-ion collisions. *Ann. Rev. Nucl. Part. Sci.* **2013**, *63*, 123–151.
2. Gale, C.; Jeon, S.; Schenke, B. Hydrodynamic modeling of heavy-ion Collisions. *Int. J. Mod. Phys. A* **2013**, *28*, 1340011.
3. Strickland, M. Anisotropic hydrodynamics: Three lectures. *Acta Phys. Pol. B* **2014**, *45*, 2355–2394.
4. Fukushima, K. Evolution to the Quark-Gluon Plasma. 2016, arXiv:1603.02340.
5. Matsui, T.; Satz, H. J/ψ Suppression by quark-gluon plasma formation. *Phys. Lett. B* **1986**, *178*, 416–422.
6. Karsch, F.; Mehr, M.T.; Satz, H. Color screening and deconfinement for bound states of heavy quarks. *Z. Phys. C* **1988**, *37*, 617–622.
7. Emerick, A.; Zhao, X.; Rapp, R. Bottomonia in the quark-gluon plasma and their production at RHIC and LHC. *Eur. Phys. J. A* **2012**, *48*, 72,
8. Nendzig, F.; Wolschin, G. Y suppression in PbPb collisions at energies available at the CERN Large Hadron Collider. *Phys. Rev. C* **2013**, *87*, 024911,
9. Zhou, K.; Xu, N.; Xu, Z.; Zhuang, P. Medium effects on charmonium production at ultrarelativistic energies available at the CERN Large Hadron Collider. *Phys. Rev. C* **2014**, *89*, 054911.
10. Hoelck, J.; Nendzig, F.; Wolschin, G. In-Medium Y-Suppression and Feed-down in UU and PbPb Collisions. 2016, arXiv:1602.00019.
11. Mocsy, A.; Petreczky, P.; Strickland, M. Quarkonia in the quark gluon plasma. *Int. J. Mod. Phys. A* **2013**, *28*, 1340012.
12. Karsch, F.; Kharzeev, D.; Satz, H. Sequential charmonium dissociation. *Phys. Lett. B* **2006**, *637*, 75–80.
13. Eichten, E.; Gottfried, K.; Kinoshita, T.; Lane, K.D.; Yan, T.M. Charmonium: Comparison with experiment. *Phys. Rev. D* **1980**, *21*, 203–233.
14. Lucha, W.; Schoberl, F.F.; Gromes, D. Bound states of quarks. *Phys. Rep.* **1991**, *200*, 127–240.
15. Brambilla, N.; Pineda, A.; Soto, J.; Vairo, A. Effective field theories for heavy quarkonium. *Rev. Mod. Phys.* **2005**, *77*, 1423–1496.
16. Brambilla, N.; Ghiglieri, J.; Vairo, A.; Petreczky, P. Static quark–antiquark pairs at finite temperature. *Phys. Rev. D* **2008**, *78*, 014017.
17. Brambilla, N.; Ghiglieri, J.; Petreczky, P.; Vairo, A. The Polyakov loop and correlator of Polyakov loops at next-to-next-to-leading order. *Phys. Rev. D* **2010**, *82*, 074019.
18. Laine, M.; Philipsen, O.; Romatschke, P.; Tassler, M. Real-time static potential in hot QCD. *J. High Energy Phys.* **2007**, *3*, 054.

19. Dumitru, A.; Guo, Y.; Strickland, M. The Heavy-quark potential in an anisotropic (viscous) plasma. *Phys. Lett. B* **2008**, *662*, 37–42.
20. Burnier, Y.; Laine, M.; Vepsalainen, M. Quarkonium dissociation in the presence of a small momentum space anisotropy. *Phys. Lett. B* **2009**, *678*, 86–89.
21. Dumitru, A.; Guo, Y.; Strickland, M. The imaginary part of the static gluon propagator in an anisotropic (viscous) QCD plasma. *Phys. Rev. D* **2009**, *79*, 114003.
22. Dumitru, A.; Guo, Y.; Mocsy, A.; Strickland, M. Quarkonium states in an anisotropic QCD plasma. *Phys. Rev. D* **2009**, *79*, 054019.
23. Margotta, M.; McCarty, K.; McGahan, C.; Strickland, M.; Yager-Elorriaga, D. Quarkonium states in a complex-valued potential. *Phys. Rev. D* **2011**, *83*, 105019.
24. Krouppa, B.; Ryblewski, R.; Strickland, M. Bottomonia suppression in 2.76 TeV Pb-Pb collisions. *Phys. Rev. C* **2015**, *92*, 061901.
25. Strickland, M.; Bazow, D. Thermal bottomonium suppression at RHIC and LHC. *Nucl. Phys. A* **2012**, *879*, 25–58.
26. Strickland, M., Thermal Upsilon(1s) and chi-b1 suppression in sqrt(s-NN) = 2.76 TeV Pb-Pb collisions at the LHC. *Phys. Rev. Lett.* **2011**, *107*, 132301.
27. W. Florkowski and R. Ryblewski, Highly-anisotropic and strongly-dissipative hydrodynamics for early stages of relativistic heavy-ion collisions. *Phys. Rev. C* **2011**, *83*, 034907.
28. Martinez, M.; Strickland, M. Dissipative dynamics of highly anisotropic systems. *Nucl. Phys. A* **2010**, *848*, 183–197.
29. Bazow, D.; Heinz, U.W.; Strickland, M. Second-order (2+1)-dimensional anisotropic hydrodynamics. *Phys. Rev. C* **2014**, *90*, 054910.
30. Nopoush, M.; Strickland, M.; Ryblewski, R.; Bazow, D.; Heinz, U.; Martinez, M. Leading-order anisotropic hydrodynamics for central collisions. *Phys. Rev. C* **2015**, *92*, 044912.
31. Bazow, D.; Heinz, U.W.; Martinez, M. Nonconformal viscous anisotropic hydrodynamics. *Phys. Rev. C* **2015**, *91*, 064903.
32. Romatschke, P.; Strickland, M. Collective modes of an anisotropic quark gluon plasma. *Phys. Rev. D* **2003**, *68*, 036004.
33. Martinez, M.; Ryblewski, R.; Strickland, M. Boost-Invariant (2 + 1)-dimensional Anisotropic Hydrodynamics. *Phys. Rev. C* **2012**, *85*, 064913.
34. Ryblewski, R.; Florkowski, W. Highly-anisotropic hydrodynamics in 3 + 1 space-time dimensions. *Phys. Rev. C* **2012**, *85*, 064901.
35. Miller, M.L.; Reygers, K.; Sanders, S.J.; Steinberg, P. Glauber modeling in high energy nuclear collisions. *Ann. Rev. Nucl. Part. Sci.* **2007**, *57*, 205–243.
36. Florkowski, W. *Phenomenology of Ultra-Relativistic Heavy-Ion Collisions*; World Scientific: Singapore, 2010.
37. Bożek, P.; Wyskiel-Piekarska, I. Particle spectra in pb-pb collisions at $\sqrt{s_{NN}} = 2.76$ tev. *Phys. Rev. C* **2012**, *85*, 064915.
38. Özönder, Ş.; Fries, R.J. Rapidity profile of the initial energy density in heavy-ion collisions. *Phys. Rev. C* **2014**, *89*, 034902.
39. Schenke, B.; Jeon, S.; Gale, C. Anisotropic flow in sqrt(s) = 2.76 TeV Pb + Pb collisions at the LHC. *Phys. Lett. B* **2011**, *702*, 59–63.
40. Petreczky, P. Quarkonium in hot medium. *J. Phys. G* **2010**, *37*, 094009.
41. Bali, G.S.; Schilling, K.; Wachter, A. Complete O(v^2) corrections to the static interquark potential from SU(3) gauge theory. *Phys. Rev. D* **1997**, *56*, 2566–2589.
42. Strickland, M.; Yager-Elorriaga, D. A parallel algorithm for solving the 3d schrodinger equation. *J. Comput. Phys.* **2010**, *229*, 6015–6026.
43. Karsch, F.; Petronzio, R. Momentum Distribution of J/psi in the Presence of a Quark - Gluon Plasma. *Phys. Lett. B* **1987**, *193*, 105–109.
44. The CMS Collaboration; Chatrchyan, S.; Khachatryan, V.; Sirunyan, A.M.; Tumasyan, A.; Adam, W.; Bergauer, T.; Dragicevic, M.; Erö, J.; Fabjan, C.; Fried, M.; et al. Suppression of non-prompt J/psi, prompt J/psi, and Y(1S) in PbPb collisions at $\sqrt{s_{NN}} = 2.76$ TeV. *J. High Energy Phys.* **2012**, *5*, 063.
45. Wöeri, H., International Workshop on Heavy Quarkonium 2014, <https://indico.cern.ch/event/278195/session/7/contribution/104/material/slides/0.pdf> (2014).



© 2016 by the authors; licensee MDPI, Basel, Switzerland. This article is an open access article distributed under the terms and conditions of the Creative Commons Attribution (CC-BY) license (<http://creativecommons.org/licenses/by/4.0/>).